Gas Contamination Effects in Variable Polarity Plasma Arc Welded Aluminum

A study was performed to characterize the effects of gas contaminants in gas lines or cylinders on variable polarity plasma arc welded 2219 aluminum

BY M. R. TORRES, J. C. MCCLURE, A. C. NUNES AND A. C. GUREVITCH

ABSTRACT. A series of variable polarity plasma arc welds were made on 0.25-in. (0.635-cm) thick 2219 aluminum sheet using carefully measured contaminant levels of oxygen, hydrogen, nitrogen and methane in both the arc and shielding gases. Porosity, asymmetric undercutting, incomplete fusion and fine extrusions at the edge of the weld were found to be associated with various levels of contamination. Many of the phenomena can be interpreted by noting that little or no true sputtering took place during the reverse polarity cycle, rather the surface tension of the weld pool was altered by even low fluxes of contaminant gases.

Introduction

Variable polarity plasma arc welding (VPPAW) has been used for aluminum welds by NASA on the space shuttle external tank with considerable success and has completely replaced GTAW in many applications.

The stiff high-velocity constricted arc of VPPAW makes the welds less sensitive to deflection by stray magnetic fields and VPPAW's lower heat input reduces workpiece distortion. Cleaning during the reverse cycle minimizes weld pool contamination from surface oxide or hydrocarbons. Welding in the keyhole or fully penetrating mode allows hydrogen to be dissolved in the thin layer of liquid aluminum surrounding the keyhole and be flushed out the backside of the weld. Thus, porosity free welds are obtained almost routinely (Ref. 1).

It has, however, been observed that occasional poor welding performance follows either arc or shielding gas cylinder changes. Incomplete fusion, a discolored arc, and undercutting are typical indications that gas cylinder contamination has occurred. The experienced welder normally detects these abnormalities during the welding process and takes corrective measures. Fuerschbach has recommended 99.999% pure arc and shielding gas for PAW and emphasizes the necessity of clean and leakproof tubing for successful welds (Ref. 2). Rough calculations, surprisingly, indicate that although VPPAW performance is clearly superior to GTAW, very low levels of gas contamination may cause porosity. For example, according to Nunes, *et al* (Ref. 3), the critical concentration of water vapor (Cwv) can be estimated if the following assumptions are approximately valid:

1) All water vapor in the weld gas is broken into gaseous hydrogen and oxygen in the welding arc.

2) All hydrogen in the weld gas dissolves in the weld metal.

3) A hydrogen content in excess of about 0.1 cm^3 per 100 grams of metal results in porosity (Ref. 4).

KEY WORDS

Gas Contaminants
Plasma Arc Welding
Aluminum Plate
Variable Polarity PAW
VPPAW
Porosity
Keyhole
Cover Pass
Oxide Films
Shielding Gas

If the weld gas volumetric flow rate is Q′, and the weld gas density is Dg, then the mass flow rate of weld gas is

$$R_g = D_g Q' \quad (1)$$

Let Cwv be the weight fraction of water vapor and Dw and Dh be the densities of water vapor and hydrogen, then the volume flow rate of hydrogen is

$$R_h = C_{wv} D_g Q' (1/D_w) (D_w/D_h) \quad (2)$$

or

$$R_h = C_{wv} (D_g/D_h) Q' \quad (3)$$

assuming the amount of water vapor contained is small.

The mass of metal absorbing the hydrogen per unit time is $D_M AV$ where D_M is the density of the metal, A is the weld cross-section area, and V is the weld speed.

Using assumption 1 above, the critical concentration Cwv of water vapor can be found from

$$C_{wv} D_g Q'/D_M AV = 10^{-3} cm^3/g \quad (4)$$

For hydrogen and argon, the plasma gas, measured at STP,

$$C_{wv} = 5AV/Q' \quad (5)$$

and for helium the shielding gas,

$$C_{wv} = 50AV/Q'$$

Representative values of A = 0.15 $in.^2$ (96.7 mm^2), V = 8 in./min (3.4 mm/s), and Q′ = 6 ft^3/h (2.83 L/min) for the argon plasma gas, 50 ft^3/h (24 L/min) for the helium shielding gas yield critical contamination levels of 1 ppm for both argon and helium.

M. R. TORRES, J. C. McCLURE and A. C. GUREVITCH are with the Metallurgy and Materials Engineering Department, University of Texas at El Paso, Tex. A. C. NUNES is with the Materials and Processes Laboratory, Marshall Space Flight Center, Ala.

Table 1—Weld Parameters

	Keyhole	Cover
Current, A	140	120
Additional Reverse Current, A	50	30
Voltage, V	31	24
Torch Speed, in./min (mm/s)	9 (3.8)	7 (2.9)
Plasma Gas Flow Rate, cfh (L/min)	5.2 (2.4)	2 (0.94)
Shield Gas Flow Rate, cfh (L/min)	40 (18.8)	40 (18.8)
Forward Polarity, ms	19	19
Reverse Polarity, ms	4	4
Orifice Diameter, in. (cm)	1/8 (0.32)	1/8 (0.32)
Electrode Diameter, in. (cm)	3/16 (0.48)	3/16 (0.48)
Source Gas Pressure, psi	50	50
Thoriated tungsten electrode, polished flat		

Consequently, a study was undertaken to determine the effects of gaseous contaminants in the arc and shielding gas during VPPA welding of aluminum alloy 2219. Similar studies of the effects of such impurities during GTAW have been conducted in the past. A review of 18 separate studies can be found in Masubuchi where levels of 400 ppm of hydrogen in the gas were needed to initiate porosity and levels of 500 ppm are needed to cause easily noticeable surface degradation (Ref. 5). Gaseous contaminants used in the present study include hydrogen, nitrogen, methane and oxygen.

Experimental Procedure

Uphill, bead-on-plate welds were made on 0.25-in.-thick 2219 T87 aluminum. A Hobart Brothers Corp. VPPAW welding machine (Model 300), including power supply and plasma controller, was used. A Marshall Space Flight Center-designed torch was obtained from the B&B Corp. of Brownsboro, Ala.; it eliminated problems sometimes associated with PAW torches such as electrode centering difficulties and cooling water leakage.

The gas flow schematic is shown in Fig. 1. All tubing was stainless steel that had been triple rinsed in methyl ethyl ketone and distilled water and blown dry with helium. Stainless steel Swagelock fittings were used throughout, and all joints were leak tested. The meters, valves and gas cylinder regulators were all stainless steel with Viton being the only nonmetal in contact with the gas.

The weld hose supplied was polymer and was a possible source of gas diffusion and hydrocarbon outgassing. The 12-ft hose was cleaned with alcohol, blown dry, and bagged before sending to Scott Specialty Gasses of Houston, Tex. Scott performed tests to determine if other gases were collected when ultrapure helium was flowed through the hose. After about ½h of purging, 2.4 ppm oxygen and 12.4 ppm hydrocarbons were found in the hose outlet stream. These are very low levels and constitute a baseline contaminant level for the present study. Throughout this paper all reported contaminant levels are in addition to these levels.

Pure argon and helium were purchased and certified to be 99.9999% pure. The same ultrapure argon and helium gas cylinders separately contaminated with 500 to 600 ppm (certified contaminant levels were known to within 5%) of hydrogen, nitrogen, methane and oxygen were also purchased. Lower contaminant levels were obtained by using Omega mixing rotameters and diluting the contaminated gases with the pure gases. Gas flow velocity was monitored using Omega electronic hot wire flow meters. The 2219 plates were solvent wiped with methyl ethyl ketone, degreased, alkali etched, brightened, rinsed in water, and blown dry prior to each test. The relative humidity was about 20% for all tests.

A total of 24 keyhole and 22 keyhole plus cover pass welds were made. Weld parameters are shown in Table 1. Plates 4 in. (10.16 cm) wide X 48 in. (122 cm) long X 0.25 in. (0.635 cm) thick were firmly bolted between two 0.5-in.(1.27-cm) thick by 12-in. (30.48-cm) wide aluminum heat sinks. The torch was moved with a motorized torch track and torch holder. Considerable effort was expended to align the workpiece and torch track parallel such that torch standoff distance would not vary greatly during welding. Torch standoff distance changes, as determined by changes in arc voltage (continuously monitored with a strip chart recorder), were less than one volt or less than about 3%.

To highlight changes in weld character when gas contaminants were used,

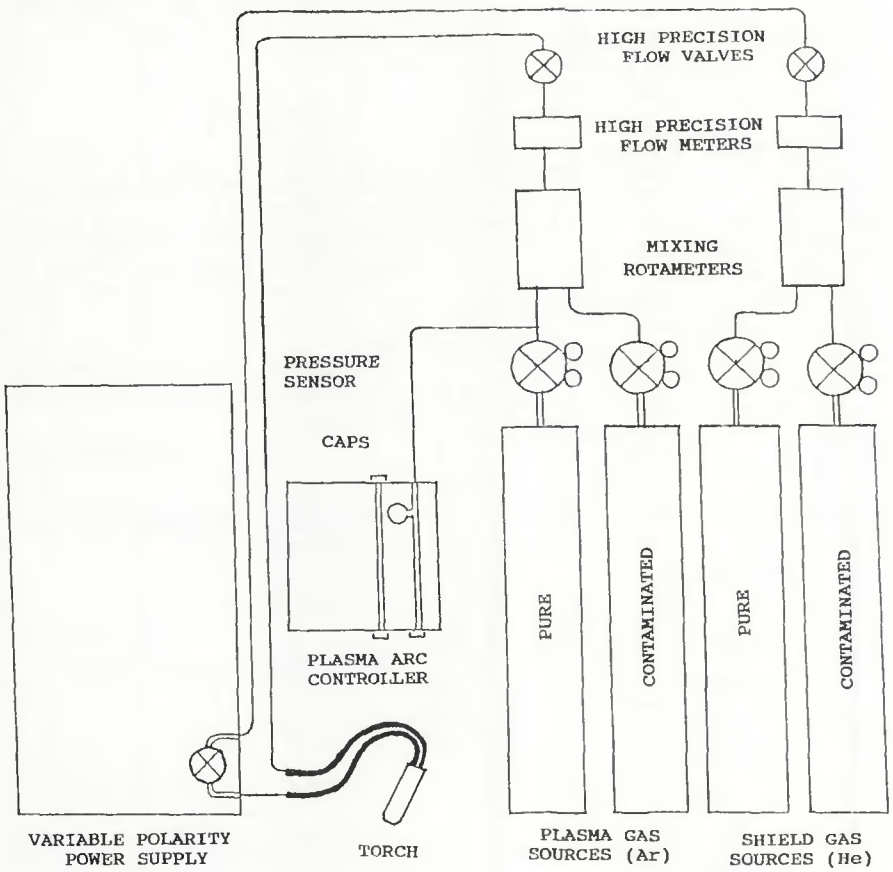

Fig. 1 — Schematic of experimental gas flow system.

welds were made as shown in Fig. 2. Welds were started in the keyhole mode with pure gas, and halfway up the workpiece the contaminants were added to either the arc or shielding gas. When the keyhole weld pass was complete, the torch was lowered, the sheet cooled, and an ultrapure cover pass weld was started midway through the pure keyhole weld. Halfway up the workpiece the gas was again contaminated. Thus, each weld sequence provided samples of pure gas keyhole, contaminated gas keyhole, pure gas keyhole plus pure gas cover, and contaminated gas keyhole plus contaminated cover welds. Gas flow velocity was kept constant to within 2% except during the approximately 3 in. (7.62 cm) of weld needed to make the changeover from pure to contaminated gases.

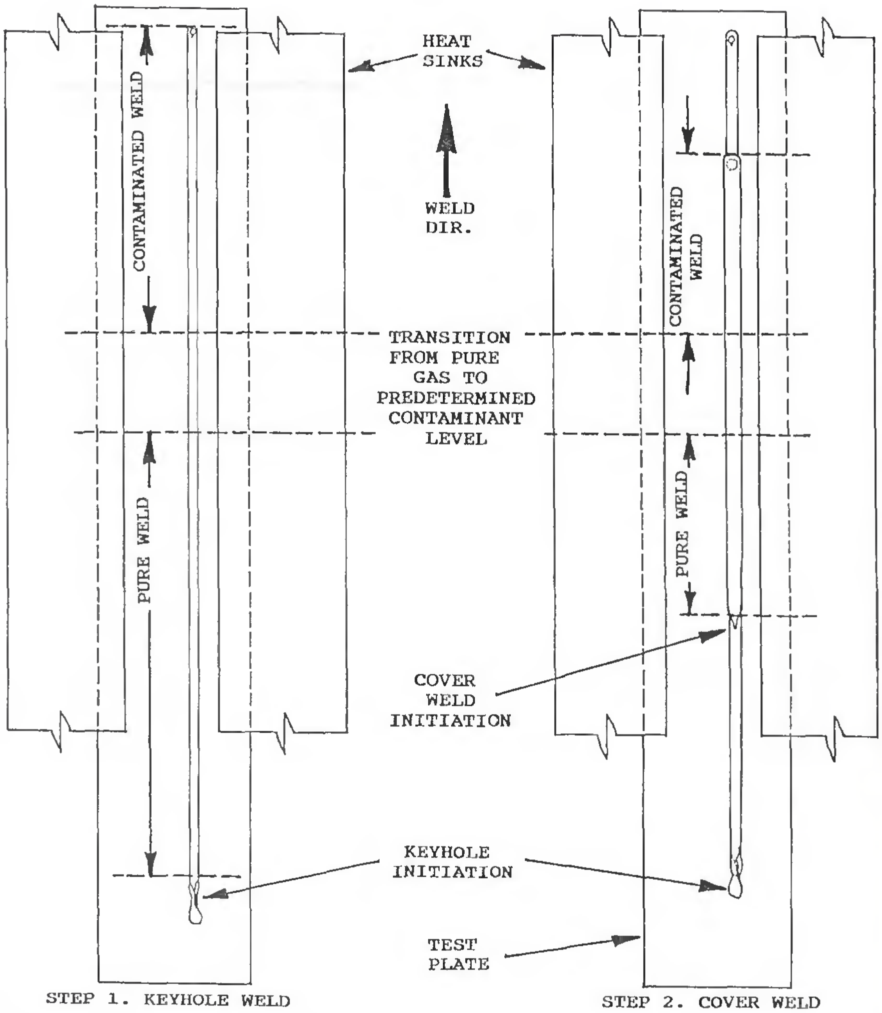

Fig. 2 — 2219 aluminum plate showing location of pure and contaminated welds and position of keyhole and cover passes.

Results and Discussion

Results for various contaminant welds are summarized in Figs. 3 and 4. Some of the effects include microporosity, incomplete fusion, undercutting, and surface rippling. Except as discussed below under porosity, keyhole and cover pass contamination produced similar results.

Porosity

Porosity can occur in the weld metal when dissolved gases are present in amounts greater than their solid solubility limits (Ref. 6). Porosity was highest for hydrogen in shielding, methane in shielding, and methane in arc contaminants. The equilibrium constant for the disassociation reaction

$$CH_4 \rightarrow C+2H_2 \quad (6)$$

is 1 at 1950 K (3050°F) and the temperature of the arc is estimated to be 15,000 K (35,540°F) (Ref. 7). These numbers suggest that ample free hydrogen is available to cause porosity. The minimal porosity in welds with high levels of hydrogen in the arc will be discussed below.

Pore analysis was conducted from 50 to 156X magnification. The majority of pores were detected along weld edges. Porosity generally took the shape of the metal grain structure in which solidification occurred. A dendritic type of grain structure resulted in elongated pores. Pores found among coarser grains were spherical in shape. Pores ranged in size from 0.04 mm (0.0016 in.) diameter to 0.14 mm (0.0055 in.) at the weld edges. The largest observed pore was found in the 500 ppm hydrogen in shielding cover pass.

More pores were always observed during the cover pass than the keyhole pass, which only penetrates about one-third of the plate. During a keyhole pass, many of the contaminants are purged out the backside of the weld bead. A cover pass, however, traps the contaminants within the metal and provides an opportunity for any supersaturated hydrogen to form pores.

Another interesting observation was the occurrence of a series of small angular shiny particles in several of the weld samples. These particles were detected primarily along the edges of the weld front side and occasionally along the weld center — Fig. 5. From analysis of weld front sides and cross-section samples, it was determined that there was a direct correlation between weld porosity and the occurrence of these features and that they occurred most often on samples with hydrogen-contaminated shielding gas with methane-contaminated arc gas. The "particles" apparently are the result of trapped gases attempting to escape out of the weld front side just as solidification occurred — Fig. 6.

Incomplete Fusion and Surface Rippling

Complete fusion was accomplished for all contaminants except for hydrogen in arc and methane in shield additions. When welding with a pure gas, the backside appears as a continuous stream of molten aluminum flowing from the keyhole to the trailing edge of the weld pool. The 250 ppm hydrogen in the arc addition, seen in Fig. 7, resulted in intermittent metal flow entraining solidified pieces of metal or oxide. Similar results, though to a lesser extent, were observed for the 100 ppm hydrogen in the arc pass. Poor wettability was also observed for methane in shielding additions. The 400 ppm methane addition resulted in an irregular surface with poor fusion on either one or both weld edges — Fig. 8.

To understand these results, certain details of the VPPA process should be

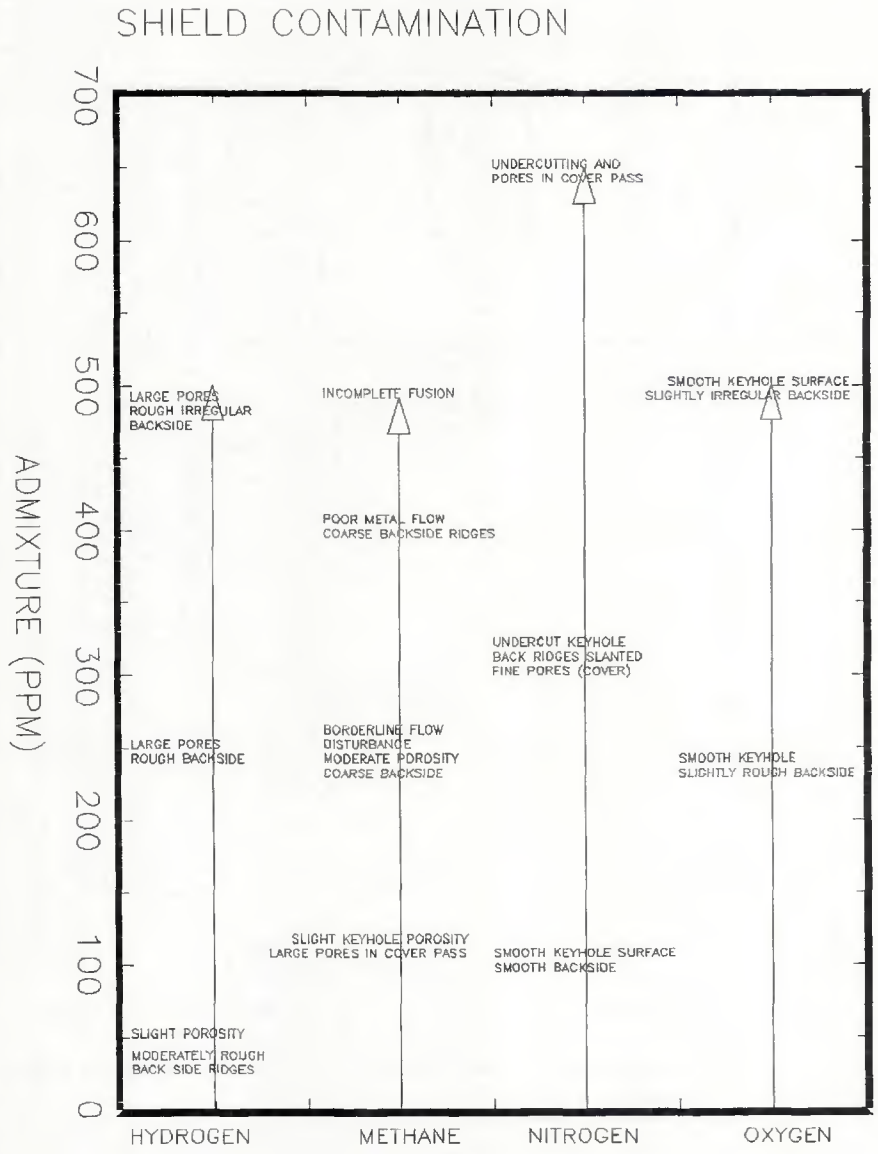

Fig. 3 — Chart shows the effects of shielding gas comtamination on the weld metal.

noted. First, there is a substantial flux of charged ions arriving at the workpiece. The number of charged (assuming single ionization) particles per unit area is given by

$$p = INf_r/vw \qquad (7)$$

where I = reverse polarity current in amperes, fr = fraction of reverse time, w = width of sputtered region, v = weld speed and N = number of charges per coulomb (6.25×10^{18}). For the conditions of these experiments, $\rho = 4.51 \times 10^{20}$ ions/cm^2. If there are 10^{15} atoms/cm^2 on the surface, species present in the arc gas at even 10 to 100 ppm (depending on the sticking coefficient) may form a stable monolayer.

Secondly, although the arc voltage is 31 V, the electrons and ions in the arc reach thermal equilibrium by collisions. As previously stated, the arc temperature is estimated to be 15,000 K in plasma welding, which is an energy of only 1.3 ev. The ions pick up an additional approximately 6 ev of energy in the cathode fall region, but their total energy is only slightly greater than the surface binding energy of aluminum oxide (3.8 ev). Data on sputter yields of such low energy ions are not available, but, for example, the yield of aluminum atoms with 100 ev (13 times the average energy of the VPPA plasma) argon ions is only 0.04 atoms/ion (Ref. 8). It thus seems unlikely that any appreciable sputter cleaning occurs.

Thirdly, convection driven by surface tension gradients in the pool will be outward and downward. The narrow pool in PAW and the large liquid range of aluminum contribute to very strong Marangoni convection. Velocities of 100 cm/s have been observed in good agreement with calculations (Ref. 9).

Since sputtering does not occur to any appreciable extent and convection can be very strong, it appears that the main effect of electrode positive (reverse) polarity is to break up surface contamination layers rather than to remove them. After break up of the roughly 6 nm surface oxide layer (Ref. 10), convection disperses the oxide fragments throughout the weld zone.

Since the equilibrium constant for ionization

$$H \rightarrow H^+ + e^- \qquad (8)$$

is 1 at 16,000 K (28,340°F) (Ref. 11), which is approximately arc temperature, most of the hydrogen in the arc gas exists as H+. These hydrogen ions are aggressive reducing agents and may remove existing oxide or new oxide that forms due to low levels of oxygen in the arc gas. As shown above, a hydrogen concentration of between 10 and 100 ppm in the arc supplies a sufficient flux of ions to remove portions of the roughly ten layers of surface aluminum oxide. Work by Goumiri on the surface tension of liquid aluminum that had been sputter cleaned with argon ions (and verified clean with Auger spectroscopy) shows an increase in surface tension from 860 mJ/m^2 to 1050 mJ/m^2 when the last two monolayers of oxide are removed (Ref. 10). Removal of portions of the aluminum oxide allows the remaining surface oxide to be distributed, by increased Marangoni convection, to the back portion of the weld bead. The oxide fragments collect along the center of the back portion of the weld bead as can be seen in Fig. 9. The incomplete fusion and minimal porosity shown in Fig. 7 can be explained by hydrogen removing portions of the surface aluminum oxide, which in turn increases the Marangoni convection and forces the remaining oxide to the root of the weld where an oxide barrier is formed between the two surfaces to be joined.

Severe surface ripples were detected for the 100 ppm hydrogen in the arc cover pass. Fig. 10A and 10B show the front surfaces of noncontaminated and 100 ppm hydrogen in arc additions, respectively. The severe ripples are again an indication of increased convection and oxide barrier formation.

Results for methane in arc additions differed from those of hydrogen in the arc in that no incomplete fusion problems were encountered. Methane in the arc is completely disassociated and the atoms are ionized by the high tempera-

ture. Equilibrium constants for $C \rightarrow C^+$ and $H \rightarrow H^+$ are 1 at 14,000 K (24,740°F) and 16,000 K (28,340°F), respectively (Ref. 11). Ionized hydrogen again removes surface oxides, but the ionized carbon will impact the surface and continuously form an undissolved layer of Al_3C_4 on the surface of the weld pool. This layer evidently prevents an increase in Marangoni convection and inhibits distribution of oxide particles to the back of the weld bead.

The temperature in the shielding gas surrounding the arc gas falls very quickly and by the edge of the shielding falls below the melting point of aluminum (Ref. 12). Methane in the shielding is largely disassociated (the equilibrium constant for $CH_4 \rightarrow C+2H_2$ is 1 at approximately 1950 K — Ref. 11) but not ionized. The atomic hydrogen again cleans away the oxide layer, but the atomic carbon evidently forms Al_3C_4 less efficiently than the ionic carbon in the arc. Thus, increased flow and distribution of oxide particles again prevent complete fusion.

At high enough concentrations, hydrogen in the shielding gas should have the same cleaning effect as the hydrogen from dissociated methane in the shielding. Higher concentrations of hydrogen are required because each molecule of methane provides twice the number of free hydrogen atoms as diatomic hydrogen. With high enough concentrations of either gas, there will be enough porosity that convection cannot purge the melt and poor welds will result.

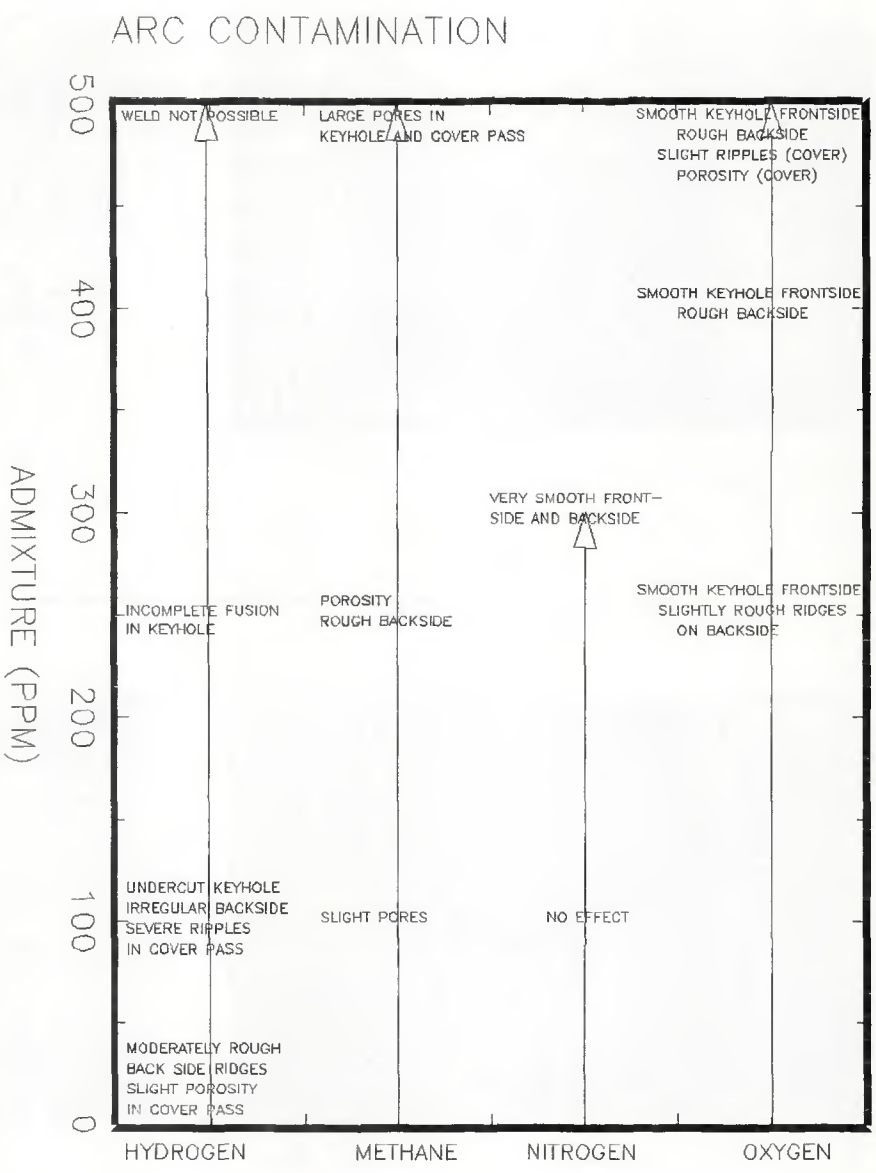

Fig. 4 — Chart shows the effects of arc gas contamination on the weld metal.

Undercutting

Asymmetric undercutting can be the result of slight arc misalignment sometimes in combination with gaseous contaminants and proved to be one of the experimental difficulties. Several welds were redone because of unacceptable undercutting. Undercutting was corrected by axially rotating the torch before the contamination sequence was initiated.

Figure 11 is a schematic of a weld when the arc is not perfectly perpendicular to the workpiece. The heat distribution into the pool will be asymmetric with greater heat on the side away from the electrode. The spatial gradient of surface tension from the center to the edge of the weld will be greater on the side away from the electrode, producing faster Marangoni convection on that side (Ref. 13). Changes in weld pool velocity can induce undercutting by Bernouli and surface tension effects and account for a depression in the faster convecting side. An estimate of the required changes in convection velocity needed to produce the observed undercut can be obtained by writing the Bernouli and surface tension terms as

$$2P = 2\rho v_o \delta v \qquad (9)$$

$$\sigma = PH \qquad (10)$$

where v_o is the liquid velocity, δ_v is the change in liquid velocity, and H is the height of the undercut. Combining Equations 9 and 10 yields

$$\delta v = \frac{\sigma}{\rho v_o H} \qquad (11)$$

For an observed undercut height of 0.79 mm (0.031 in.) and an estimated liquid velocity of 100 cm/s, δ_v must be of the order of 40 cm/s to produce the undercut.

Except for the higher concentrations of hydrogen in the arc and methane in the shielding, which caused disastrous welds, clear evidence of contamination induced undercutting was observed with 650 ppm and 325 ppm nitrogen in the shielding and 100 ppm hydrogen in the arc. Figure 12 shows three cross-sections which were made respectively with pure gas, 650 ppm nitrogen in shielding, and pure gas. These sections were made on one pass and are only a few inches apart. This procedure was repeated several times and proved to be a pattern. Undercuts in passes prior to secondary passes can introduce defects such as porosity or incomplete fusion into a weld.

The undercutting observed with nitrogen and hydrogen is caused when these gases preferentially enter one side of the weld pool and raise the surface tension by either scavenging oxygen (in

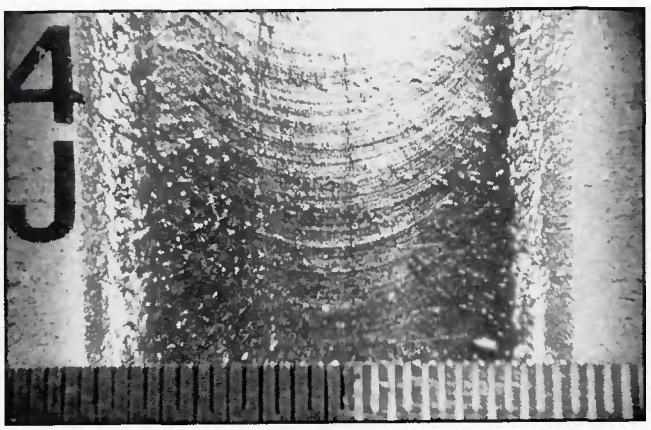

Fig. 5 — Bubbles on surface of 500 ppm methane in arc cover pass. 8X magnification. Ruler divisions: 1/64 in. (0.4 mm).

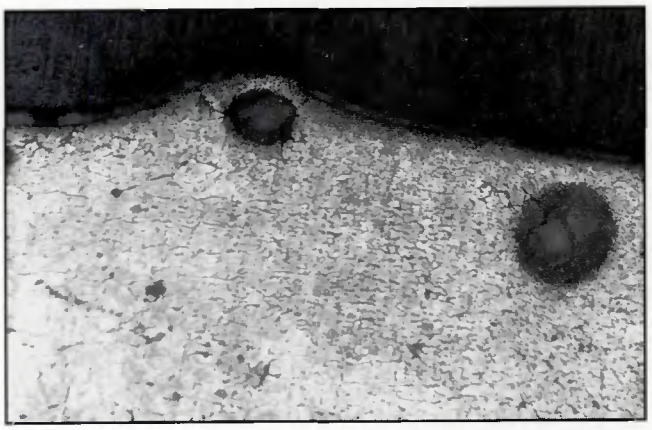

Fig. 6 — Weld cross-section showing formation of bubbles on weld surface. 125X magnification.

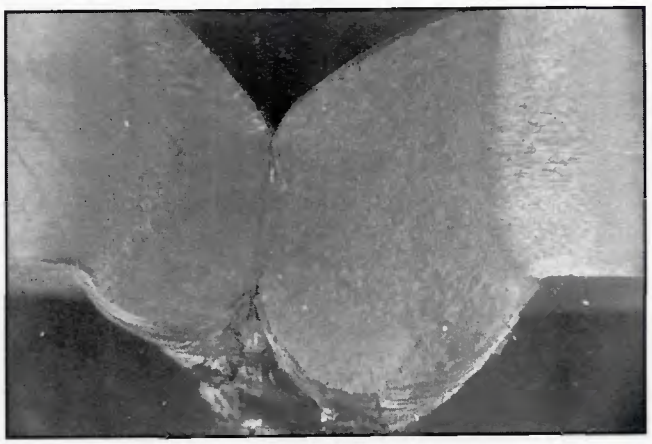

Fig. 7 — Weld cross-section of 250 ppm hydrogen in arc showing incomplete fusion. 8X magnification.

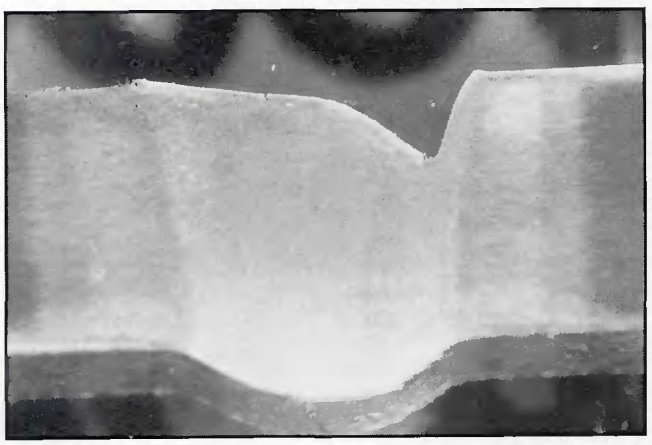

Fig. 8 — Weld cross-section of 400 ppm methane in shield showing poor fusion. 8X magnification.

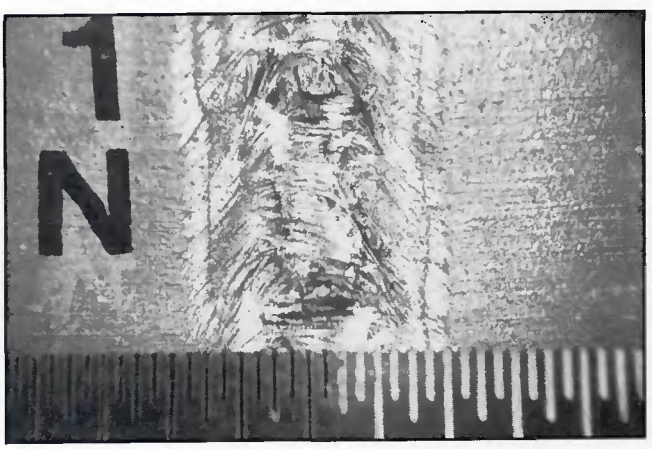

Fig. 9 — Weld backside of 100 ppm hydrogen in arc showing aluminum oxide collection at weld center. 8X magnification. Ruler divisions: 1/64 in. (0.4 mm).

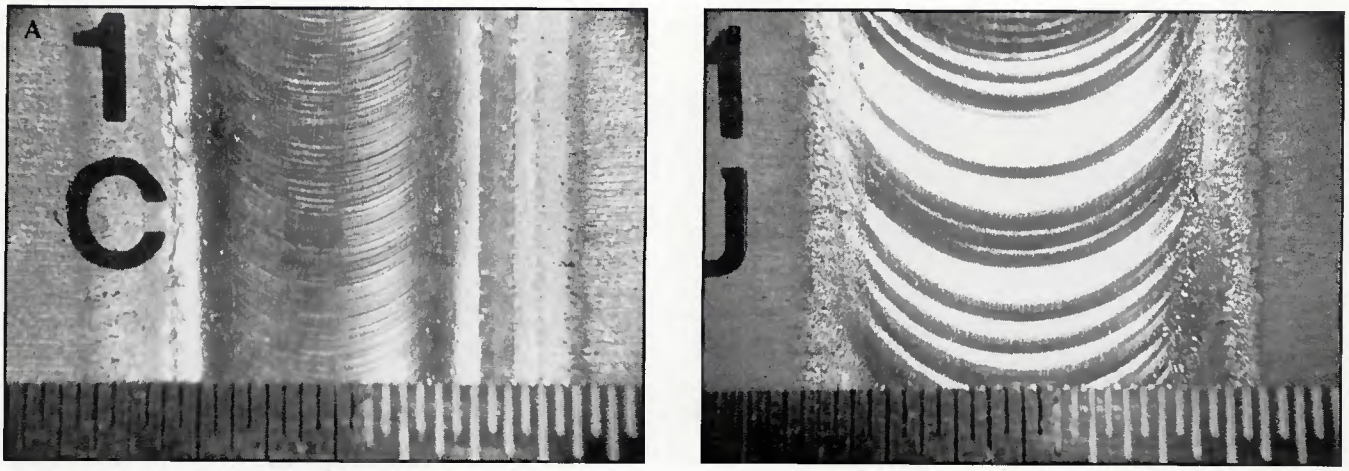

Fig. 10 — A — Weld front surface of pure cover pass. 8X magnification. Ruler divisions: 1/64 in. (0.4 mm); B — weld front surface of 100 ppm hydrogen in arc cover pass. Note severe ripples. 8X magnification. Ruler divisions: 1/64 in. (0.4 mm).

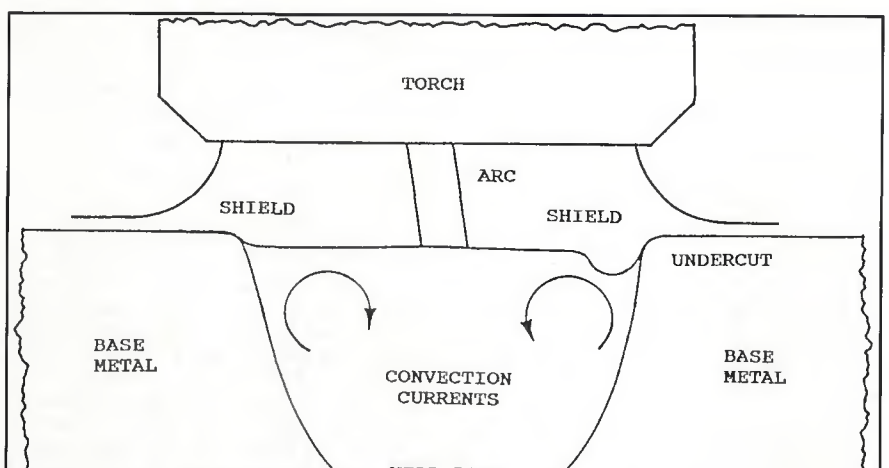

Fig. 11 — Schematic showing formation of weld undercut.

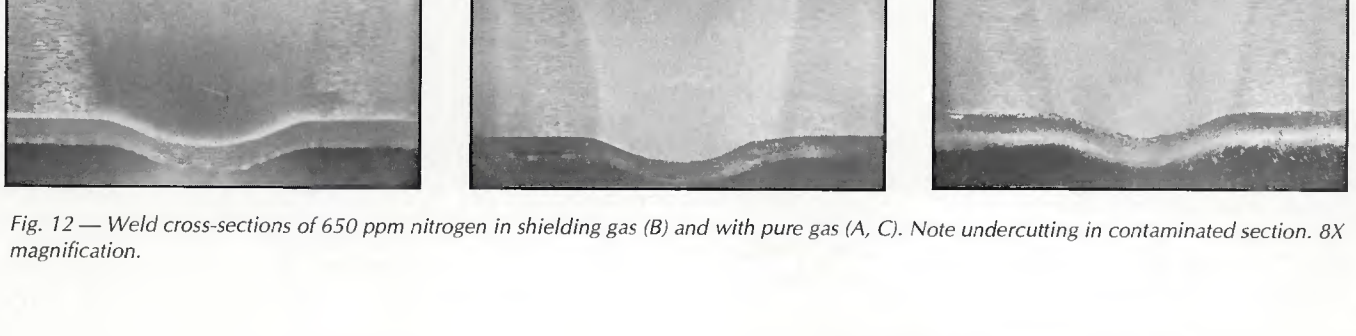

Fig. 12 — Weld cross-sections of 650 ppm nitrogen in shielding gas (B) and with pure gas (A, C). Note undercutting in contaminated section. 8X magnification.

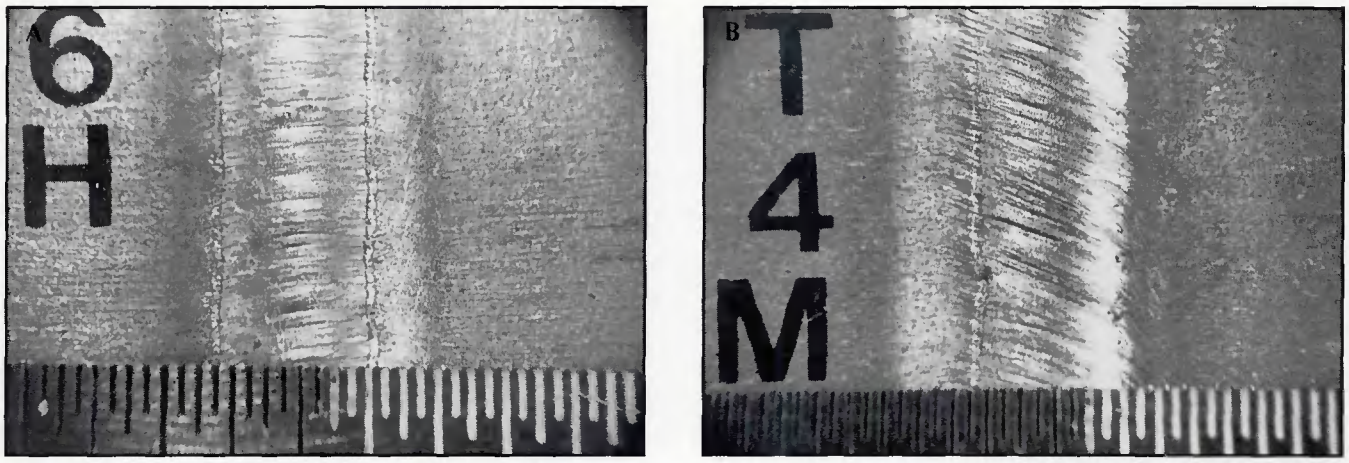

Fig. 13 — A — Weld backside of a pure gas with ridges perpendicular to weld direction. 8X magnification. Ruler divisions: 1/64 in. (0.4 mm); B — weld backside of 650 ppm nitrogen in shielding gas with ridges slanted toward undercut side. 8X magnification. Ruler divisions: 1/64 in. (0.4 mm).

the case of hydrogen) or nitrogen absorption (Ref. 14) on that side of the weld. The surface tension gradient ($d\sigma/dT$) increases and raises the convection rate on that side of the weld. Contaminated gases can be preferentially absorbed on one side of a weld due to a slight torch misalignment. Note that the pure gas pictures in Fig. 12 show a slight undercut from torch misalignment that was amplified by the contamination.

Asymmetric undercutting can also be detected from the weld backside by the orientation of the backside ridges and is also a consequence of asymmetric heat flow into the weld during keyhole welds. Figure 13A shows the backside of a good weld with backside ridges perpendicular to the weld direction. Figure 13B shows the angled ridges of an undercut weld. The ridges slant downward toward the undercut side. If more heat is delivered to one side of the weld, the metal flowing out the back of the keyhole will be hotter and solidify later than the liquid on the cooler side. Undercutting during a keyhole pass may be covered up by later nonpenetrating passes, but the angled ridges remain as an indication of keyhole undercutting.

The contaminants also affected pilot arc operation. With no contaminants present, the pilot arc operated as a continuous light purple flame, a color that is associated with argon ionization. With contaminants of about 500 ppm, the pilot arc appeared to "die" out or change in coloration, and current flow was intermittent, especially with hydrogen, in the weld torch. During methane in arc tests, pilot arc coloration changed to a fine green while oxygen produced a white arc. Nitrogen affected the pilot arc less noticeably, but coloration did change from purple to a light blue. This visual technique is especially effective in detecting contamination problems before arc-to-workpiece transfer occurs.

Conclusions

The experimental process described was an effective method of characterizing the effects of gaseous contaminants on the appearance of VPPAW 2219 aluminum. An efficient gas mixing and line purging sequence is essential in performing tests of this kind. Results of the study revealed the following:

1) Hydrogen levels of 25 ppm in the shielding gas produce microporosity and the associated surface features caused by bubbles of gas reaching the surface just as it solidifies.

2) Methane concentrations of 100 ppm produced fine porosity.

3) Nitrogen concentrations of 300 ppm were required to produce fine porosity and undercutting.

4) Oxygen contamination of 250 ppm can be detected by rough backsides on keyhole welds.

5) The main effect of the reverse current cycle of the VPPAW process is to break up surface oxides rather than remove them by sputtering.

6) Incomplete fusion is a result of removal of portions of the thin oxide on the aluminum surface by either disassociated or ionized hydrogen. The remaining oxide is free to move and forms wetting barriers at the back of the weld pool.

7) Asymmetric undercutting is a result of slight arc misalignment, sometimes in combination with gas contaminants, which may preferentially enter one side of the weld pool and increase Marangoni flow on that side.

8) Asymmetric undercutting can be detected on the backside of the weld bead by observing the orientation of weld ridges.

Acknowledgments

The support of the National Aeronautics and Space Administration through Marshall Space Flight Center under contract NAS8-37425 is gratefully acknowledged. Scott Specialty Gasses of Houston, Tex., provided much helpful advice about gas handling and provided critical gas purity measurements.

References

1. Nunes, A. C., Bayless, E. O., and Wilson, W. A. 1984. The variable polarity plasma arc welding process: its application to the space shuttle external tank — second interim report. NASA Technical Memorandum TM-86482, Marshall Space Flight Center, Huntsville, Ala.

2. Fuerschbach, P. W. 1985. Plasma arc welding, equipment, installation, and process control. National Technical Information Services. Albuquerque, N. Mex., Sandia National Laboratories.

3. Nunes, A. C., Bayless, O. E., Jones, C. S., Munafo, P. M., Biddle, A. P., and Wilson, W. A. 1983. The variable polarity plasma arc welding process: its application to the space shuttle external tank — first interim report. NASA Technical Memorandum TM-82532. Huntsville, Ala., Marshall Space Flight Center.

4. Cibula, A. 1967. Gases in cast and wrought metals. Twenty-first autumn course, Institution of Metallurgists. Eds. O. Kubaschewski, A. Cibula and D. C. Moore, *Gases and Metals*, American Elsevier Publishing Co.

5. Masubuchi, K. 1972. Integration of NASA-sponsored studies on aluminum welding. NASA Contractor Report CR-2064. Massachusetts Institute Of Technology, Cambridge, Mass.

6. Devletian, J. H., and Wood, W. E. Factors affecting porosity in aluminum welds. Welding Research Council Bulletin 290.

7. Gittens, T. E. 1988. Plasma arc processes — an overview. Proceedings International Power Beam Conference. Eds. E. A. Metsbower and D. Hauser, pp. 11–21. ASM

International, Materials Park, Ohio.

8. Behrisch, R. 1981. *Topics In Applied Physics*, Vol. 47, Springer Verlag, New York, N.Y.

9. Correa, S. M., and Sundell, R. E. 1986. A computational and experimental study of the fluid flow in weld pools. Proceedingsof the Third Conference on Modeling of Casting and Welding Processes. Eds. S. Kou and R. Mehrabian, pp. 211–227. TMS.

10. Goumiri, L., and Joud, J. C. 1982. Auger electron spectroscopy study of aluminum-tin liquid system. *Acta Metallurgica* 30, pp. 1397–1405.

11. CRC. *Handbook Of Tables For Applied Engineering Science*, 2nd Edition.

12. Metcalfe, J. C., and Quigley, M. B. C. 1975. Heat transfer in plasma — arc welding. *Welding Journal* 53(3): 99-s to 102-s.

13. Wang, Y. H., and Kou, S., 1986. 3-D weld pool convection — a dimensionless presentation. Proceedings of the Third Conference on Modeling of Casting and Welding Processes. Eds. S. Kou and R. Mehrabian, pp. 197–209. TMS.

14. Engler, S., and Ellerbrok, R. 1974. Measurements of the surface tension of liquid aluminum alloys. *Giessereiforschung* 26(1): 43–48.

WRC Bulletin 336
September 1988

Interpretive Report on Dynamic Analysis of Pressure Components—Fourth Edition

This fourth edition represents a major revision of WRC Bulletin 303 issued in 1985. It retains the three sections on pressure transients, fluid structure interaction and seismic analysis. Significant revisions were made to make them current. A new section has been included on Dynamic Stress Criteria which emphasizes the importance of this technology. A new section has also been included on Dynamic Restraints that primarily addresses snubbers, but also discusses alternatives to snubbers, such as limit stop devices and flexible steel plate energy absorbers.

Publication of this report was sponsored by the Subcommittee on Dynamic Analysis of Pressure Components of the Pressure Vessel Research Committee of the Welding Research Council. The price of WRC Bulletin 336 is $20.00 per copy, plus $5.00 for postage and handling. Orders should be sent with payment to the Welding Research Council, Suite 1301, 345 E. 47th St., New York, NY 10017.

WRC Bulletin 357
September 1990

Calculation of Electrical and Thermal Conductivities of Metallurgical Plasmas

By G. J. Dunn and T. W. Eagar

There has been increasing interest in modeling arc welding processes and other metallurgical processes involving plasmas. In many cases, the published properties of pure argon or helium gases are used in calculations of transport phenomena in the arc. Since a welding arc contains significant quantities of metal vapor, and this vapor has a considerably lower ionization potential than the inert gases, the assumption of pure inert gas properties may lead to considerable error. A simple method for calculating the electrical and thermal conductivities of multicomponent plasmas is presented in this Bulletin.

Publication of this report was sponsored by the Welding Research Council. The price of WRC Bulletin 357 is $20.00 per copy, plus $5.00 for U.S. or $10.00 for overseas postage and handling. Orders should be sent with payment to the Welding Research Council, 345 E. 47th St., New York, NY 10017.

WRC Bulletin 339
December 1988

Development of Tightness Test Procedures for Gaskets in Elevated Temperature Service
By A. Bazergui and L. Marchand

In this report, different elevated temperature gasket tightness test procedures are compared. A two-tier test approach, involving aging of the preloaded gasket in a kiln followed by a short duration tightness test was evaluated. The procedures were evaluated using spiral-wound gaskets with two different fillers: a mica-graphite filler and an asbestos filler.

Publication of this report was sponsored by the Subcommittee on Bolted Flanged Connections of the Pressure Vessel Research Committee of the Welding Research Council. The price of WRC Bulletin 339 is $16.00 per copy, plus $5.00 for postage and handling. Orders should be sent with payment to the Welding Research Council, 345 E. 47th St., Suite 1301, New York, NY 10017.

WRC Bulletin 344
June 1989

This Bulletin contains two reports covering three-dimensional finite element analysis of 45-deg lateral branch pipe models.

(1) Three-Dimensional Finite Element Analysis of PVRC 45-Degree Lateral Model 4 (d/D = 0.5, D/T = 40) under Out-of-Plane Moment Loading on Branch Pipes
By P. P. Raju

(2) Three-Dimensional Finite Element Analysis of 45-Degree Lateral Model 2 (d/D = 0.5, D/T = 10) under Out-of-Plane Moment Loading on the Branch Pipe
By P. P. Raju

Publication of these reports was sponsored by the Joint Task Group on Laterals of the Subcommittee on Piping, Pumps and Valves, and the Subcommittee on Reinforced Openings of the Pressure Vessel Research Committee of the Welding Research Council. The price of WRC Bulletin 344 is $16.00 per copy, plus $5.00 for U.S., or $8.00 for overseas, postage and handling. Orders should be sent with payment to the Welding Research Council, 345 E. 47th St., Room 1301, New York, NY 10017.

WRC Bulletin 346
August 1989

WFI/PVRC Moment Fatigue Tests on 4 × 3 ANSI B16.9 Tees

By G. E. Woods and E. C. Rodabaugh

The Markl-type fatigue test data presented in this report have been needed for a number of years to establish i-factors (SIFs) for forged tees with d/D ratios between 0.5 and 1.0 that conform to the ANSI B16.9 standard. These new data will provide improved design rules for both nuclear and industrial piping systems.

Publication of this report was sponsored by the Subcommittee on Piping Pumps and Valves of the Pressure Vessel Research Committee of the Welding Research Council. The price of WRC Bulletin 346 is $25.00 per copy, plus $5.00 for U.S. and $10.00 for overseas postage and handling. Orders should be sent with payment to the Welding Research Council, Room 1301, 345 E. 47th St., New York, NY 10017.